NIH Public Access
Author Manuscript
Clin Cancer Res. Author manuscript; available in PMC 2015 July 15.

Published in final edited form as:
Clin Cancer Res. 2014 July 15; 20(14): 3884–3895. doi:10.1158/1078-0432.CCR-13-0556.

FANCD2 is a Potential Therapeutic Target and Biomarker in Alveolar Rhabdomyosarcoma Harboring the PAX3/FOXO1 Fusion Gene

Mamata Singh[1,¥], **Justin Leasure**[1,¥], **Christopher Chronowski**[1,¥], **Brian Geier**[2], **Kathryn Bondra**[1], **Wenrui Duan**[1], **Lauren Hensley**[1], **Miguel Villalona-Calero**[1], **Ning Li**[1], **Anthony Vergis**[1], **Raushan Kurmasheva**[2], **Changxian Shen**[2], **Gary Woods**[2], **Nikhil Sebastian**[1], **Denise Fabian**[1], **Rita Kaplon**[1], **Sue Hammond**[2], **Kamalakannan Palanichamy**[1], **Arnab Chakravarti**[1], and **Peter J. Houghton**[2]

[1]Wexner Medical Center at The Ohio State University, Arthur G. James Comprehensive Cancer Center and Richard L. Solove Research Institute

[2]Nationwide Children's Hospital, Columbus, OH

Abstract

Purpose—Alveolar rhabdomyosarcoma that harbors the PAX3/FOXO1 fusion gene (t-ARMS) is a common and lethal subtype of this childhood malignancy. Improvement in clinical outcomes in this disease is predicated upon the identification of novel therapeutic targets.

Experimental Design—Robust mouse models were used for *in vivo* analysis, and molecular studies were performed on xenografts treated in parallel. Two independent patient sets (n=101 and 124) of clinically-annotated tumor specimens were used for analysis of FANCD2 levels and its association with clinical and molecular characteristics and outcomes.

Results—Our xenograft studies reveal a selective suppression of FANCD2 by m-TOR kinase inhibition and radiosensitization of the t-ARMS line only. In the initial patient set, we show FANCD2 transcript levels are prognostic in univariate analysis, and are significantly associated with metastatic disease and that the co-presence of the translocation and high expression of FANCD2 is independently prognostic. We also demonstrate a significant and non-random enrichment of mTOR-associated genes that correlate with FANCD2 gene expression within the t-ARMS samples, but not within other cases. In the second patient set, we show that on a protein level, FANCD2 expression correlates with PAX3/FOXO1 fusion gene and is strongly associated with phospho-P70S6K expression in cases with the fusion gene.

Conclusions—Our data demonstrate that FANCD2 may have a significant role in the radiation resistance and virulence of t-ARMS. Indirectly targeting this DNA repair protein, through mTOR inhibition, may represent a novel and selective treatment strategy.

Corresponding Author: Peter J. Houghton[2], PhD. Director, Center for Childhood Cancer, The Research Institute, Nationwide Children's Hospital, 700 Children's Drive, Columbus, OH 43205, Ph. 614 355 2670, Fx. 614 355 2927, Peter.Houghton@nationwidechildrens.org.
¥Indicates authors contributed equally to this work.

Conflicts of Interest: None of the authors of this report have any conflicts of interest to report.

NIH-PA Author Manuscript
NIH-PA Author Manuscript
NIH-PA Author Manuscript

NIH-PA Author Manuscript

NIH-PA Author Manuscript

NIH-PA Author Manuscript

Keywords

rhabdomyosarcoma; PAX3/FOXO1 fusion gene; FANCD2; mTOR; radioresistance

Introduction

There are approximately 350 new cases of pediatric rhabdomyosarcoma (RMS) diagnosed per year in the United States (1). Despite progress made in this disease, control of the primary site is still a major source of treatment failure, as 2/3 of the relapses observed in Intergroup RMS Study-IV (n=888) were local-regional (2), suggesting an inherent resistance to radiotherapy in this childhood malignancy. Alveolar RMS (ARMS) is the most biologically aggressive subtype of this disease, which confers a 5-year overall survival of less than 50% (10–30% for metastatic disease) compared to the more favorable, embryonal subtype (ERMS), which confers a 73% 5-year overall survival. Driving the poor prognosis in ARMS is the presence of the t(2;13)(q35;q14) translocation observed in 60–70% of ARMS, which gives rise to the chimeric transcription factor, PAX3-FOXO1, a constitutively active oncogene that significantly alters gene expression and confers an 8% four-year overall survival to patients with this disease (3). The impact of PAX3/FOXO1 fusion gene is so pervasive that it appears to segregate RMS into two distinct molecular and clinical groups: those harboring this translocation (t-ARMS) and all other subtypes, including ERMS, non-translocated ARMS, and ARMS harboring the PAX7/FOXO1 fusion gene (though its clinical virulence is less clear) (4). Clinical outcome improvements in the treatment of t-ARMS will have the greatest impact upon the pediatric RMS population as a whole. Further, lowering radiation doses required to eradicate gross and microscopic disease reduces the likelihood and severity of acute and long-term toxicity, as total dose and treated-volume are directly related to their development, especially in children (5–6).

Recently, Yu and colleagues demonstrated that the conditional knockout of mTOR resulted in the loss of the Fanconi anemia group D2 (FANCD2) mRNA and protein expression in hemopoietic stem and progenitor cells (7). This resulted in a significant gain of DNA double-strand breaks and cell sensitivity when exposed to DNA cross-linking chemotherapeutic agents. This result suggested that mTOR inhibition leads to loss of FANCD2 expression, leading to more accumulated DNA damage and hence cell kill. Interestingly, the activation of the mTOR/Akt pathway appears to be prognostic in pediatric rhabdomyosarcoma, with high levels of phospho-Akt and phospho-P70S6K (and other intermediates) having significant associations to poorer overall and progression-free survival in patient samples; findings which prompted preliminary *in vitro* testing with mTOR inhibition (via CCI-779) that resulted in significant reductions in cell growth (8).

New inhibitors have been developed to inhibit both TORC1 and TORC2 complexes (9–10) and may more closely approximate the effects of mTOR knockdown than the first-generation of mTOR inhibitors, which primarily inhibit TORC1. AZD8055 (AstraZeneca, United Kingdom), a novel ATP-competitive inhibitor of mTOR kinase activity, acts as a dual TORC1 and TORC2 inhibitor and was used in our study. AZD8055 was recently tested within the Pediatric Preclinical Testing Program, causing only modest growth inhibition

NIH-PA Author Manuscript

NIH-PA Author Manuscript

NIH-PA Author Manuscript

against some of the RMS lines (11), with otherwise non-toxic effects on mice. Further *in vivo* testing of AZD8055 in this setting revealed that indeed there was a drug-induced down regulation of FANCD2 through mTOR inhibition. Specifically, FANCD2 gene transcripts were reduced via the blockade of the mTORC1-S6K1 pathway (12). With these data taken collectively, we postulated that a complete mTOR blockade via pharmacologic means could potentially enhance radiation sensitivity in pediatric RMS.

The FANCD2 protein in humans is encoded by the FANCD2 gene and belongs to Fanconi anemia complementation group (FANC) and is a crucial mediator of this DNA repair pathway (13). Mutations in any one of the genes comprising this complementation group can lead to the development of Fanconi's anemia, often resulting in elevated cancer risks, congenital abnormalities, and bone marrow failure. Mutations within FANCD2 result in most severe phenotype (14). Clinically, patients with FA also display hypersensitivity toward agents that create DNA interstrand crosslinks (ICLs), including many chemotherapeutic drugs as well as ionizing radiation (IR) (15–16). There is also growing experimental evidence suggesting that the FA pathway plays a role in the repair of spontaneously-generated DNA double strand breaks (DSBs) as well (17).

In this report we tested the efficacy of concurrent mTOR kinase inhibition (in the hope to suppress FANCD2 expression via AZD8055 administration) and radiotherapy using an *in vivo* model that robustly recapitulates tumor biology and clinical radiation therapy delivery. We further analyzed the pharmacologic impact of AZD8055 on mTOR signaling during the response to radiotherapy as well as the expression and functional dynamics of FANCD2 in xenograft specimens collected in parallel to this preclinical screen. We then validated the importance of FANCD2 in radiation resistance in RMS using siRNA-based knockdown clonogenic survival studies. Lastly, we explored the clinical significance of FANCD2 levels as a biomarker in pediatric rhabdomyosarcoma using two independent, clinically-annotated patient sets.

Materials and Methods

Xenograft lines and mice

The xenograft lines used for the preclinical testing experiments (obtained from the Pediatric Preclinical Testing Program, Nationwide Children's Hospital, Columbus, Ohio) were two rhabdomyosarcoma (RMS) lines: Rh18 (embryonal) and Rh30 (alveolar) which were propagated and grown in mouse flanks as previously described (18). These two lines express the two major RMS genotypes: Rh30 (t-ARMS-Rh30) expresses the fusion transcription factor PAX3-FOXO1, while Rh18 (ERMS-Rh18) does not. Further, these RMS xenograft lines were selected for the current study because they were not exposed to cytotoxic agents prior to their harvesting from patients and direct engraftment into mice (19). CB17SC *scid*$^{-/-}$ female mice (Taconic Farms, Germantown NY), were used to propagate subcutaneous tumors.

NIH-PA Author Manuscript

NIH-PA Author Manuscript

NIH-PA Author Manuscript

Mouse treatment with AZD8055 and XRT and endpoints

Mice bearing each xenograft line were dosed orally with 1mg/mL AZD8055 at 5–10- and 20 mg/kg of body weight for 21 consecutive days beginning on study day 1, as previously described (11). Thereafter, body weights were measured weekly for dose calculation. Mice received fractionated flank-irradiation treatments in clinically-relevant 2-Gy daily doses as previously described using our proprietary mouse-flank irradiation device (18,20). For mice receiving concurrent therapy, radiation was given 2–4 hours after drug administration on days 8–12; irradiation treatment resumed on days 15–19 after a two-day break (reflecting the weekends off of typical treatment courses). The treatment schedule is summarized in Supplemental Figure 1A. Mice receiving concurrent treatment were treated with AZD8055 for one week prior to radiation, as at least four days were required for the suppression of FANCD2 (12), due to the relatively long half-life of the protein. Further, mice were monitored daily for skin reaction starting on day 15 from the first day of irradiation treatments through day 35. A numeric grade is given based on a rating system according to the severity of the reaction detailed in Supplementary Figure 1B. Dose density, complete response (CR) rates, recurrence rates, 12-week failure rates, event-free survival, and treatment related events (as previously described) (18) were recorded. To quantify radiosensitization impact, an enhancement ratio, [(%failure-free rate with XRT+drug)/(dose density with XRT+drug)]/[(%failure-free rate with XRT-alone)/(dose density with XRT-alone)] was used. A ratio of 1.0 signifies no enhancement.

Protein lysate extraction, Western blot and quantification

Tumors collected from mouse xenografts and flash frozen in liquid nitrogen were homogenized via mortar and pestle. The prepared tissue was then transferred to a cell lysis solution containing 1% protease inhibitor cocktail (PIC) [Sigma #P8340], 1% phosphatase inhibitor cocktail 2 [Sigma #P5726], 1% phosphatase inhibitor cocktail 3 [Sigma #P0044], and 1x PMSF in T-Per Tissue Protein Extraction Reagent [Thermo Scientific #78510]. The extracted protein concentrations from the resulting samples were then assessed using a BCA protein estimation kit (Pierce). From lysis samples representing tumors from mice that had undergone the same treatment, equivalent amounts of proteins were pooled into a combined sample for use in Western blot analysis. Protein from cells maintained *in vitro* without antibiotics were also extracted using the aforementioned cell lysis solution.

To quantify differences in protein levels, immunoblots were imaged using Bio-Rad's VersaDoc™ MP 4000 System and software (Bio-Rad, Hercules, CA). Relative density values (Intensity/mm^2) of blots for FANCD2 and Beta Actin were determined for the 0Gy, 2Gy, 4Gy, and 6Gy XRT Alone and XRT+AZD8055 samples using the Volume Rect Tool and Volume Analysis Report provided by the software. For each sample, a normalization value was determined by dividing the FANCD2 density by the Beta Actin density. This was performed for two separate immunoblot experiments. Standard deviation values were determined for each sample's normalized values. Each normalized value was then renormalized relative to the 0Gy XRT Alone control and plotted.

NIH-PA Author Manuscript

NIH-PA Author Manuscript

NIH-PA Author Manuscript

FANCD2 foci staining and counting system

The FA triple staining immunofluorescence (FATSI) method using formalin-fixed paraffin embedded (FFPE) tissues has been previously described (21). FFPE tumor tissue was cut at 4 microns, placed on positively-charged slides and stained with hematoxylin and eosin. Additional sections for immunofluorescence staining were placed in a 60°C oven for one hour, cooled, deparaffinized, and rehydrated through xylenes and graded ethanol solutions to water in standard fashion. Antigen retrieval was performed by placing slides in Dako's TRS antigen retrieval solution (Dako, Carpenteria, CA) in a calibrated vegetable steamer (Black and Decker) at 94°C for 25 minutes. Slides then were placed on a Dako Autostainer for automated staining. The tissue sections were incubated with a primary antibody cocktail of rabbit polyclonal FANC-D2 antibody (Novus Biologicals, Littleton, CO) at a dilution of 1:1000 and a monoclonal anti-Ki67 mouse antibody (Dako, Carpenteria, CA) at a dilution of 1:150, for one hour at room temperature. Sections then were co-incubated with a secondary antibody (FITC conjugated to anti-rabbit IgG and Alexa fluor 594 donkey anti-mouse IgG, Invitrogen, Carlsbad, CA) at 1:1000 for one hour at room temperature. All rinses were performed on the autostainer with TBST. The sections were mounted on glass slides using a 4′ 6-diamidino-2-phenylindole (DAPI)–containing embedding medium (Vysis Dapi 1, Abbott Laboratories, Downers Grove, IL). FANCD2 foci negative cells (PD220 or PD20) and foci positive cells (MCF-7 or FA corrected PD220 or FA corrected PD20) were used as controls on the sample slide during the procedure. The slides were analyzed under a Nikon E-400 fluorescence microscope. Cells with three or more bright green foci in the nuclei were scored as FANCD2-positive, and three similar fields (at 100X magnification) of cells were enumerated for each time point.

siRNA knockdown

In vitro transfections were carried out via INVITROGEN's Lipofectamine RNAiMAX reverse transfection procedure. The true transfection group was transfected using equal parts of two FANCD2 siRNAs provided by SIGMA-ALDRICH: SASI_Hs01_00137854 and SASI_Hs02_00307032. The negative control group was transfected using SIGMA-ALDRICH's MISSION siRNA Universal Negative Control #1. All transfections took place in T-25 tissue culture flasks. Cells were initially plated at approximately 40–50% confluence per flask. The flasks were incubated for a total of 48 hours post-transfection at 37 °C, 5% CO_2 before receiving irradiation and immediate plating for clonogenic survival analysis.

Clonogenic survival assay

Rh30 and Rh18 in vitro cells lines (also obtained from the PPTP) were both separated into three groups: control, negative (scrambled) siRNA, and FANCD2 siRNA. The plated cells were allowed to grow into colonies for 14 days before being stained with 0.05% crystal violet and counted. The 0Gy control plates for each group were used to calculate a plating efficiency as defined in Franken, et al. 2006 Nature Protocols.

Patient sets

The initial set consisted of 101 publicly available clinically-annotated pediatric rhabdomysarcoma specimens with Affymetrix U133_Plus 2.0 Array. CEL files from a

NIH-PA Author Manuscript

NIH-PA Author Manuscript

NIH-PA Author Manuscript

previously published report (4). The second set consists of 124 clinically-annotated pediatric rhabdomyosarcoma patient core samples that comprise the tissue microarray slides available from the Children's Oncology Group banking protocol for soft tissue sarcomas (COG D9902). The PAX/FOXO1 fusion status was known for the majority of cases.

Statistical Methods

The log-rank test was used in univariate comparisons of survival times (event-free in mice and overall survival in patient cases), and Cox-regression analysis was used in the multivariate analysis (backward step-wise Wald). Actuarial outcome rates and factor distributions between groups were determined using the Fisher's exact test. Spearman rank was used for determining the correlation between factors. Statistical analysis was performed using SPSS software.

Gene Expression Analytical Methods

101 RMS samples arrayed by Affymetrix U133 Plus 2.0 platform were downloaded from Array Express (4) website. The chips were processed by RMA with background adjustment and then quantile normalized via using Matlab ® Statistics toolbox. All analyses described herein were performed at a gene level. The gene level data was created using the Gene Set Enrichment Analysis (GSEA) application. An individual gene expression level was derived from maximum of all probes that mapped to a particular gene. For the molecular similarity analysis of RMS: Non-negative matrix factorization, a technique to elucidate global molecular patterns (22), was applied to the 3000 most variable genes as determined by coefficient of variation. GSEA settings: 1000 phenotype permutations were performed to assess the level of significance for gene set member rank distribution in FANCD2 defined signal-to-noise profile. Other algorithm settings were set to default. The reported GSEA statistics, in addition to p-values, were false-discovery-rate (FDR), family-wise error rate (FWER), and normalized enrichment score rank (NES rank) (20).

Immunohistochemistry

Paraffin-embedded sections (5-μm thick) were deparaffinized in xylene and rehydrated through an ethanol series. Slides were placed in a pressure cooker with Tris-EDTA buffer (pH 9.0) and heated for 10 minutes at 97°C to unmask antigen epitopes. Slides were then incubated in distilled water for 5 min at room temperature. Endogenous peroxidase activity was quenched by treatment with 3% hydrogen peroxide in absolute methanol for 30 minutes. Slides were washed in PBS containing 0.025% Tween 20 and incubated in normal blocking serum (Vectastain Elite ABC kit, Vector Laboratories, Burlingame, CA) for 60 minutes. After washing in PBS, slides were incubated with the primary antibodies overnight. Tissue sections were washed in PBS with 0.025% Tween 20, and immunostaining was performed using a species-specific biotinylated secondary antibody, avidin/biotinylated horseradish peroxidase complex, and substrate-chromogen mixture (Vectastain Elite ABC kit). Immunoreactivity was visualized using Vector DAB (brown color) peroxidase substrate as a chromogen. After washing with distilled water, the sections were dehydrated in a graded series of ethanol followed by xylene and mounted with VectaMount permanent mounting media (Vector Laboratories). The antibodies used for labeling were FANCD2, p-AKT (Ser493), and p-P70S6K (Thr389) (Cell Signaling) at 1:300, 1:100, and 1:100

NIH-PA Author Manuscript

NIH-PA Author Manuscript

NIH-PA Author Manuscript

dilutions, respectively. Scoring the staining intensity was based on a two-tiered system: with 2+ signifying intense nuclear staining throughout the tumor specimen; while a score of 1+ indicated less-intense or patchy staining throughout the tumor specimen. Samples with no staining received a score of 0. The scores were assessed while blinded from all clinical data. When there were samples with multiple cores that were assigned different scores, the most common score was the assigned score for the patient case.

Results

Preclinical screen of concurrent radiotherapy and AZD8055

We previously reported the results of our pilot study, in which the t-ARMS-Rh30 demonstrated an increased resistance to radiotherapy alone, that the dose density of 59–60 Gy/cc resulted in 12-week treatment failure rates of 78% versus 25% with Rh30 and ERMS-Rh18, respectively (18). In a dose escalation study (using 5, 10 and 20 mg of AZD8055 at radiation doses of 10 and 20 Gy), we observed that the addition of AZD8055 to XRT (after a one-week pre-treatment with daily AZD8055 alone; see Supplemental Table S1 for treatment schedule) resulted in a selective sensitization of the Rh30 line. With a mean XRT dose-density of 27 Gy/cm^3, the 12-week failure rate of Rh30-bearing mice improved to 4/15 (27%). For the Rh18 group, this rate was 8/15 (53%) at a mean dose density of 44 Gy/cm^3. Thus, the radiosensitivity enhancement factor of AZD8055 towards Rh30 was 7.3, whereas with Rh18 this ratio was 0.83 when comparing with the previous results of radiotherapy alone ($p<0.001$, Fisher's exact; a ratio of 1.0 signifies no enhancement), Supplemental Table S2.

Based on the results of the dose-escalation study, groups of 10 mice were subjected to either no treatment, AZD8055 alone for 21 consecutive days (10 mg/Kg via gavage), XRT alone (20 Gy in 10 fractions in 2 weeks), or combined treatment (AZD8055 10 mg/Kg + 20 Gy in 10 fractions with concurrent treatment lasting for two weeks after one week of AZD8055 alone). The addition of AZD8055 to radiotherapy resulted in an improvement in event-free survival rate in the Rh30-bearing mice (median EFS of 67 days in XRT-alone versus >91 days in the combined arm, $p=0.009$, log-rank), but did not impact the outcome in Rh18. (Figure 1A and 1B). Rh18 responded favorably to 20 Gy alone, with little change in outcome when the drug was added. Mice bearing the Rh30 line and receiving only 20 Gy alone had a propensity to become cachectic and develop distant metastases, resulting in early removal from study and suggesting these xenografts were under treated and remained viable to metastasize. The use of drug alone inhibited xenograft growth for about 2–3 weeks, but then it resumed as previously observed (11). There were no treatment-related deaths and the skin reaction severity of 20Gy and 30Gy with and without AZD8055 had similar average maximum intensities and recovery times (Supplementary Figures S1A, B).

FANCD2 expression and function after radiation treatments with/without mTOR kinase inhibition

In parallel with the previously mentioned preclinical murine screening, 3–5 flank xenografts (per time-point) were harvested 30–60 minutes following daily 2-Gy fractions, at cumulative doses of 2, 4, 6 and 12 Gy. Xenografts that displayed recurrence in mice receiving

NIH-PA Author Manuscript

NIH-PA Author Manuscript

NIH-PA Author Manuscript

cumulative doses 20 or 30 Gy in daily 2Gy fractions were harvested as well. To account for tumor regional heterogeneity and necrosis, samples from mice receiving equivalent treatment were combined in equal protein proportions and assessed via Western blotting. Figure 2A and 2B reveals a more pronounced drug action in t-ARMS-Rh30. Without AZD8055, there is a brisk upregulation of FANCD2 at 2Gy and 4Gy, followed by a gradual decline at subsequent timepoints. In the presence of the drug, the upregulation of FANCD2 after 2 Gy is significantly blunted and the protein is entirely absent in later timepoints. Closer inspection of the immunoblot analysis at a cumulative dose of ≥4 Gy reveals not only blockade of the downstream TORC1/TORC2 phosphorylated/activated species, but also loss of total Akt, P70S6K and mTOR (Supplementary Figure S2), suggesting a comprehensive shutdown of these pro-survival pathways. Within the ERMS-Rh18 line, the effect of AZD8055 is less pronounced. FANCD2 protein expression is not as briskly upregulated in the early fractions of radiotherapy, nor are these levels as strikingly abrogated in the presence of this drug. The protein and phospho-protein levels of TORC1/TORC2 signaling cascade remain more stable throughout the XRT treatment course with or without co-administration of AZD8055 as well.

To determine if the FANCD2 function of the two xenograft lines was affected differently by AZD8055 in these treatment settings, we performed a FANCD2 functional foci staining assay on formalin-fixed paraffin embedded thin sections of the xenografts harvested at the parallel timepoints of our immunblot analysis (Figure 2C and 2D). Consistent with the preclinical screen outcomes and immunoblot analysis, the addition of AZD8055 appears to preferentially alter/diminish the function of FANCD2 in t-ARMS-Rh30. At all cumulative timepoints, the presence of AZD8055 significantly reduces the FANCD2 activity within this xenograft line. Further, as observed at the protein expression level, the greatest difference in activity between the Rh30 xenografts treated with radiation alone and radiation plus drug occurs at the 4 Gy time-point, where AZD8055 appears to lower the percent of positively-staining nuclei from 25% to 8%. In the ERMS-Rh18 line, there is a modest gain in activity of FANCD2 in the 2Gy and 4Gy, but the impact of AZD8055 on this activity appears to have a random/variable effect from timepoint to timepoint, with a lower magnitude of differences between treatment regimens.

Clonogenic survival assay

To verify the importance of FANCD2 in the radiation responsiveness of these two xenograft lines and to rule out any potential “off-target” effects of AZD8055, we performed clonogenic survival assays of Rh18 and Rh30 cells *in vitro*, with and without direct, transient siRNA inhibition of FANCD2 expression (Supplementary Figure S3). Compared to untreated and non-targeted controls, the knockdown of FANCD2 in both Rh18 and Rh30 resulted in increased sensitivity to radiation. Rh30 demonstrated a broader shoulder than Rh18 and AZD8055 had a greater impact at the higher dose-per-fraction ranges.

The impact of FANCD2 transcript expression in clinically-annotated pediatric rhabdomyosarcoma specimens

The patient characteristics and prognostic factors of this set are summarized in Supplementary Table S3 (Gene Expression Set) These data reflected an adequate

NIH-PA Author Manuscript

NIH-PA Author Manuscript

NIH-PA Author Manuscript

representative RMS population. Further, based on the clinical stage and grouping as well as histology, it can be estimated that 95 out of the 101 patients would have received radiotherapy as all or part of their local therapy component. The mRNA levels were analyzed as a continuous variable as well as a quartile rank. Interestingly, in a univariate analysis, the mRNA expression levels were prognostic with the upper quartile having the worst overall survival time at a mean of 5.1 years, while the lowest quartile had a mean survival of 8.7 years and the mid-quartiles yielded two subsets, ranging between 5.5 and 6.5 years (Figure 3A, p=0.043, log-rank). Quartile FANCD2 expression directly correlated with Stage 4 disease (CC: 0.170, p=0.046, Spearman), and had a trend in association with the PAX3/FOXO1 fusion gene (CC: 0.122, p=0.111, Spearman). Because of the observed differences in FANCD2 expression and activity after radiotherapy in t-ARMS-Rh30 and ERMS-Rh18, we sought to determine if FANCD2 had a differential prognostic impact on these respective clinical subtypes. When stratified by histology, the top quartile rank of FANCD2 transcript expression was found to be adversely prognostic in the ARMS group, but not the ERMS group (Figure 3B). When stratified by the PAX3/FOXO1 fusion gene status, the top quartile rank of FANCD2 transcript expression was found to be adversely prognostic in the fusion-positive group, but not the fusion negative group (Figure 3C). Cases with both high FANCD2 and the PAX3/FOXO1 fusion gene had the worst outcome (mean 2.9 years) compared to the dually-negative subgroup which had the most favorable outcome (mean 9.9 years; p=0.045, pair-wise log-rank). The group with one positive marker had an intermediate outcome (mean 6.6 years). To test if dual presence of PAX3/FOXO1 fusion gene and high FANCD 2 mRNA expression was an independent prognostic variable, a Cox multivariate analysis was performed on this set (Table 1). In addition to stage 4 (metastatic disease) and presence of the PAX3/FOXO1 fusion gene, the co-expression of this oncogene and high FANCD2 was independently and adversely prognostic [HR: 3.2; 95% confidence interval: 1.5–7.5, p=0.033], after accounting for histology, nodal stage, primary tumor site, tumor size, FANCD2 expression and other fusion statuses.

The relationship between mTOR signaling, PAX3/FOXO1 fusion gene and FANCD2 in gene expression profiles

We hypothesized that mTOR interacting genes are more likely to be associated with FANCD2 mRNA in the setting of PAX3/FOXO1 fusion gene versus those RMS without this translocation, based on the selective efficacy of AZD8055 in Rh30 and observations of FANCD2 activity and expression after several 2 Gy daily fractions of radiotherapy. The Ingenuity Pathway Analysis Interactive Pathway Builder (Ingenuity® Systems, www.ingenuity.com) was used to discover a panel of genes with experimentally observed direct interaction, either up- or down-stream of mTOR, and are summarized in Supplementary Table S4. These mTOR-associated genes were then analyzed using a supervised k-means clustering with respect to FANCD2 mRNA within both the PAX3/FOXO1 fusion-positive and -negative subsets using Matlab® Statistics toolbox. Three distinct mRNA populations arose from clustering within both groups characterized primarily by high, low and intermediate FANCD2 transcript levels. Fusion-positive samples with “high” FANCD2 (n=18) had 4.3-fold higher FANCD2 mRNA levels than those with “low” status (n=3); similarly, RMS without the PAX3/FOXO1 fusion gene demonstrated a 4.8 fold change between “high” (n=18) and “low” (n=7) groups (the results of the k-means clustering

NIH-PA Author Manuscript

NIH-PA Author Manuscript

NIH-PA Author Manuscript

are visualized in Figures 4A and B). The groups with intermediate levels were not analyzed. To test our mTOR-FANCD2 hypothesis, we applied gene set enrichment analysis (23) by using a convenient desktop application maintained by the Broad Institute (24). We found by sample permutation that PAX3/FOXO1-fusion-positive RMS with “low” FANCD2 mRNA demonstrated direct enrichment of mTOR-associated genes, while in samples with “high” FANCD2 mRNA, there was an inverse enrichment of mTOR-associated genes. While weakly significant (p=0.07, FDR=0.68, FWER=1, NES rank=410), this clearly displayed a non-random enrichment and the plot can be visualized in Figure 4C. Interestingly, those RMS with no recorded translocation demonstrated a random rank distribution of mTOR interacting genes (Figure 4D) with respect to the FANCD2 mRNA signal-to-noise profile and was not statistically significant (p=0.54, FDR=0.61, FWER=1, NES rank=3,760). While the data is correlative, it demonstrates that there is a potential mechanistic relationship between mTOR and FANCD2 that may be specific to the molecular framework that the PAX3/FOXO1 fusion gene creates.

Assessment of FANCD2 protein expression in the COG D9902 tissue microarray

There were 121 cases in which at least one core was adequate for immunohistochemical staining of FANCD2, p-P70S6K (Thr 389) and p-Akt (Ser 493). Most cases had 2–3 individual cores within the array. There were 71 (59%) ARMS cases, 47 ERMS (39%) cases, and one case each of mixed histology, undifferentiated, and RMS not otherwise specified. Of the 121, only 94 cases had complete survival data. For complete demographics and clinical prognostic factors in these 94 patients, please refer to Supplementary Table S3 (TMA Set). All but two cases would have received radiotherapy as part of the multi-modality treatment course. There were no cases in which the FANCD2 score was 0, but there were three distinct staining patterns observed in both p-P70S6K and p-Akt. A Spearman rank screen of molecular and clinical markers across all cases demonstrated that FANCD2 was significantly correlated with p-P70S6K and the presence of the PAX3/FOXO1 fusion gene (Table 2; All Cases), but no other clinical or molecular factors. While there was a trend in the FANCD2/p-Akt correlation, pAkt and p-P70S6K were strongly correlated, suggesting that concordant TORC1/TORC2 activation frequently occurred in these samples. Within the cases harboring the PAX3/FOXO1 fusion gene (n=30), there was a strong correlation between FANCD2 and p-P70S6K (correlation coefficient: 0.60; $p<0.001$, Table 2; Fusion Positive Cases). However, FANCD2 is not significantly correlated with p-Akt expression, consistent with our previous observation that FANCD2 is regulated primarily via TORC1 signaling in the t-ARMS-Rh30 cell line (25). In the cases which do not harbor the fusion gene (n=65), FANCD2 was not correlated with p-P70S6K nor p-Akt (Table 2; Fusion Negative Cases). The scoring breakdown, stratified by fusion gene status, is presented in Supplementary Table S5.

Assessment of FANCD2’s survival associations in the PAX3/FOXO1 fusion gene-positive cases proved to be difficult in this patient set. There were only 6/22 cases of fusion-positive cases with complete survival data that had low (1+) FANCD2 scores. Further, with 64% of the cases censored, within this set, identification of factors which can have subtle impacts on survival is difficult to identify as well.

NIH-PA Author Manuscript

NIH-PA Author Manuscript

NIH-PA Author Manuscript

Discussion

Our preclinical and clinical data suggest that FANCD2 has a significant role in resistance to radiotherapy and potentially overall survival in t-ARMS. Further, our data demonstrate that FANCD2 expression and activity may be modulated by mTOR signaling (specifically by TORC1 signaling) within this disease type. Thus, mTOR inhibition during radiotherapy may represent an effective radiosensitization strategy in the clinic setting. This finding is significant in that it is the first time a specific potential mediator of treatment resistance has been identified in the t-ARMS subtype. Improving the efficacy of radiotherapy in t-ARMS, which have a high rate of local failure and mortality, could have a profound impact in pediatric RMS, as this is the most common and lethal form of this disease. The significance of FANCD2 in ERMS and those RMS without the PAX3 fusion gene is less clear. While the knockdown of FANCD2 in vitro resulted in a sensitization of the ERMS-Rh18, this line was already significantly more sensitive to radiotherapy than the t-ARMS-Rh30 (as is seen clinically), suggesting that greater vulnerability to ionizing radiation that is present within this xenograft line and supersedes the impact of FANCD2.

Based upon the expression and activity dynamics of FANCD2 within our preclinical screen, it appears that this is a radiation response protein, especially in the early phases of fractionated treatment. It was surprising, then, that the presence of elevated expression (at the transcript level) in patient specimens was prognostic within the t-ARMS subgroup. It is worthwhile to note that the majority of rhabdomyosarcoma patients undergo induction chemotherapy prior to their local therapy. Thus, at the time of tissue collection, there are already active compensatory mechanisms to address DNA damage brought upon by systemic agents with cross-linking induction capabilities (namely, cyclophosphamide). It is well established that DNA damage and replicative stress induces the expression and activity of FANCD2 (26). It may very well be that determining FANCD2 expression status at the time of surgery provides insight into the tumor’s ability to resist all DNA-directed cytotoxic therapy in the treatment course of rhabdomyosarcoma (including radiation) and thus may explain this impact on overall survival. It is further tempting to speculate that if this resistance mechanism in t-ARMS is significantly driven by mTOR activity and is unique to these tumor cells, there could be a rationale for mTOR kinase inhibition prior to or during XRT in patients with these tumors and subsequently improving the therapeutic ratio. Because of the consistency of the preclinical testing and correlative clinical findings and the dichotomous nature of the PAX3/FOXO1 oncogene, which segregates RMS into two distinct disease subtypes, clinically and molecularly, we feel these data may be applicable to the RMS population as a whole, despite only testing two xenograft lines. These suppositions, of course, warrant further investigation.

Finally, the results of these experiments demonstrate the utility and feasibility of our approach in testing novel agents and other potential radiosensitizers *in vivo* while identifying a possible mechanism of resistance which has clinical relevance. This represents the first time a systemic agent has been given with radiotherapy within the Pediatric Preclinical Testing Program model, as well. We are able to use large numbers of mice, to generate sufficient samples for statistically-powered outcomes studies and numerous biospecimens for molecular studies. It is the anticipation of our group to continue these preclinical screens,

NIH-PA Author Manuscript

NIH-PA Author Manuscript

NIH-PA Author Manuscript

to find efficacious sensitizers, and elucidate the molecular mechanisms behind pediatric tumor radiobiology in parallel. This approach is especially important in childhood cancer research, given the relative rarity of the many solid tumors which arise in this patient population.

Supplementary Material

Refer to Web version on PubMed Central for supplementary material.

Acknowledgments

The authors thank Christopher Pelloski for his contributions to this work, and Irene Snyder for her assistance in preparing this manuscript for publication. The authors also thank Natalie Beeler for her assistance in obtaining the COG D9902 tissue micro-array and corresponding data. Lastly, the authors express their gratitude for AstraZeneca in supplying the AZD8055 for the experiments.

Grant Support.

This work was supported through: 1P50CA127001 (CEP); NO1-CM-42216 (PJH), CA77776 (PJH), RC2CA148190 (AC), R01CA108633 (AC), from the National Cancer Institute; a Hope On Wheels Programmatic Grant from the Hyundai Corporation of North America; and a grant from the Veterans of Foreign Wars of Ohio, Sarcoma Seed Funding Program, and The Ohio State University Comprehensive Cancer Center (AC).

References

1. Ognjanovic S, Linabery AM, Charbonneau B, Ross JA. Trends in childhood rhabdomyosarcoma incidence and survival in the United States, 1975–2005. Cancer. 2009; 115:4218–26. [PubMed: 19536876]
2. Davicioni E, Anderson MJ, Finckenstein FG, Lynch JC, Qualman SJ, Shimada H, et al. Molecular classification of rhabdomyosarcoma--genotypic and phenotypic determinants of diagnosis: a report from the Children's Oncology Group. Am J Pathol. 2009; 174:550–64. [PubMed: 19147825]
3. Sorensen PH, Lynch JC, Qualman SJ, Tirabosco R, Lim JF, Maurer HM, et al. PAX3-FKHR and PAX7-FKHR gene fusions are prognostic indicators in alveolar rhabdomyosarcoma: a report from the children's oncology group. J Clin Oncol. 2002; 20:2672–9. [PubMed: 12039929]
4. Williamson D, Missiaglia E, de Reynies A, Pierron G, Thuille B, Palenzuela G, et al. Fusion gene-negative alveolar rhabdomyosarcoma is clinically and molecularly indistinguishable from embryonal rhabdomyosarcoma. J Clin Oncol. 2010; 28:2151–8. [PubMed: 20351326]
5. Ishida Y, Sakamoto N, Kamibeppu K, Kakee N, Iwai T, Ozono S, et al. Late effects and quality of life of childhood cancer survivors: Part 2. Impact of radiotherapy. Int J Hematol. 2010; 92:95–104. [PubMed: 20577841]
6. Armstrong GT, Stovall M, Robison LL. Long-term effects of radiation exposure among adult survivors of childhood cancer: results from the childhood cancer survivor study. Radiat Res. 2010; 174:840–50. [PubMed: 21128808]
7. Guo, F.; Lie, J.; Du, W.; Zhang, S.; Liu, W.; Thomas, G., et al. mTOR Regulates DNA Damage Response of Hematopoietic Stem and Progenitor Cells Through Modulation of Fanconi Anemia Core Complex. 53rd ASH Annual Meeting and Exposition; 2011;
8. Petricoin EF 3rd, Espina V, Araujo RP, Midura B, Yeung C, Wan X, et al. Phosphoprotein pathway mapping: Akt/mammalian target of rapamycin activation is negatively associated with childhood rhabdomyosarcoma survival. Cancer Res. 2007; 67:3431–40. [PubMed: 17409454]
9. Russell RC, Fang C, Guan KL. An emerging role for TOR signaling in mammalian tissue and stem cell physiology. Development. 2011; 138:3343–56. [PubMed: 21791526]
10. Wander SA, Hennessy BT, Slingerland JM. Next-generation mTOR inhibitors in clinical oncology: how pathway complexity informs therapeutic strategy. J Clin Invest. 2011; 121:1231–41. [PubMed: 21490404]

NIH-PA Author Manuscript

NIH-PA Author Manuscript

NIH-PA Author Manuscript

11. Houghton PJ, Gorlick R, Kolb EA, Lock R, Carol H, Morton CL, et al. Initial testing (stage 1) of the mTOR kinase inhibitor AZD8055 by the pediatric preclinical testing program. Pediatr Blood Cancer. 2012; 58:191–9. [PubMed: 21337679]
12. Shen C, Oswald D, Phelps D, Cam H, Pelloski CE, Pang Q, et al. Regulation of FANCD2 by the mTOR Pathway Contributes to the Resistance of Cancer Cells to DNA Double-Strand Breaks. Cancer Res. 2013; 73:3393–401. [PubMed: 23633493]
13. Kim H, D'Andrea AD. Regulation of DNA cross-link repair by the Fanconi anemia/BRCA pathway. Genes Dev. 2012; 26:1393–408. [PubMed: 22751496]
14. Kalb R, Neveling K, Hoehn H, Schneider H, Linka Y, Batish SD, et al. Hypomorphic mutations in the gene encoding a key Fanconi anemia protein, FANCD2, sustain a significant group of FA-D2 patients with severe phenotype. Am J Hum Genet. 2007; 80:895–910. [PubMed: 17436244]
15. Deans AJ, West SC. DNA interstrand crosslink repair and cancer. Nat Rev Cancer. 2011; 11:467–80. [PubMed: 21701511]
16. Dextraze ME, Gantchev T, Girouard S, Hunting D. DNA interstrand cross-links induced by ionizing radiation: an unsung lesion. Mutat Res. 2010; 704:101–7. [PubMed: 20079875]
17. Houghtaling S, Newell A, Akkari Y, Taniguchi T, Olson S, Grompe M. Fancd2 functions in a double strand break repair pathway that is distinct from non-homologous end joining. Hum Mol Genet. 2005; 14:3027–33. [PubMed: 16135554]
18. Kaplon R, Hadziahmetovic M, Sommerfeld J, Bondra K, Lu L, Leasure J, et al. The application of radiation therapy to the Pediatric Preclinical Testing Program (PPTP): results of a pilot study in rhabdomyosarcoma. Pediatr Blood Cancer. 2013; 60:377–82. [PubMed: 22692929]
19. Houghton JA, Houghton PJ, Webber BL. Growth and characterization of childhood rhabdomyosarcomas as xenografts. Journal of the National Cancer Institute. 1982; 68:437–43. [PubMed: 6950170]
20. Lu L, Bondra K, Gupta N, Sommerfeld J, Chronowski C, Leasure J, et al. NanoDots Dosimetry for RS 2000 X-Ray Biological Irradiator. Int J Radiat Biol. 2013
21. Duan W, Gao L, Zhao W, Leon M, Sadee W, Webb A, et al. Assessment of FANCD2 nuclear foci formation in paraffin-embedded tumors: a potential patient-enrichment strategy for treatment with DNA interstrand crosslinking agents. Transl Res. 2012
22. Brunet JP, Tamayo P, Golub TR, Mesirov JP. Metagenes and molecular pattern discovery using matrix factorization. Proc Natl Acad Sci U S A. 2004; 101:4164–9. [PubMed: 15016911]
23. Subramanian A, Tamayo P, Mootha VK, Mukherjee S, Ebert BL, Gillette MA, et al. Gene set enrichment analysis: a knowledge-based approach for interpreting genome-wide expression profiles. Proc Natl Acad Sci U S A. 2005; 102:15545–50. [PubMed: 16199517]
24. Subramanian A, Kuehn H, Gould J, Tamayo P, Mesirov JP. GSEA-P: a desktop application for Gene Set Enrichment Analysis. Bioinformatics. 2007; 23:3251–3. [PubMed: 17644558]
25. Shen C, Oswald D, Phelps D, Cam H, Pelloski CE, Pang Q, et al. Regulation of FANCD2 by the mTOR pathway contributes to the resistance of cancer cells to DNA double strand breaks. Cancer Res. 2013
26. Sobeck A, Stone S, Hoatlin ME. DNA structure-induced recruitment and activation of the Fanconi anemia pathway protein FANCD2. Mol Cell Biol. 2007; 27:4283–92. [PubMed: 17420278]

NIH-PA Author Manuscript

NIH-PA Author Manuscript

NIH-PA Author Manuscript

STATEMENT OF TRANSLATIONAL RELEVANCE

In our report we provide insight into the virulence of one of the most devastating cancer diagnoses in children, alveolar rhabdomyosarcoma which harbors the PAX3/FOXO1 fusion gene. Our data suggest that within this disease subtype, FANCD2 plays a role in its resistance to treatment, imparts a poorer overall survival rate when elevated in these tumors, and is specifically modulated by mTOR activation. Utilizing the robust xenograft models of the Pediatric Preclinical Testing Program, we show that the kinase inhibition of mTOR results in a selective radiosensitization of this alveolar rhabdomyosarcoma subtype via abrogation of FANCD2 expression and activity. We then show the potential clinical importance of FANCD2 through the analysis of over 200 clinically-annotated patient tumor specimens at the transcript and protein levels. This may represent a unique and exploitable treatment strategy to improve the local control rates after radiotherapy and overall survival in children diagnosed with this disease.

NIH-PA Author Manuscript
NIH-PA Author Manuscript
NIH-PA Author Manuscript

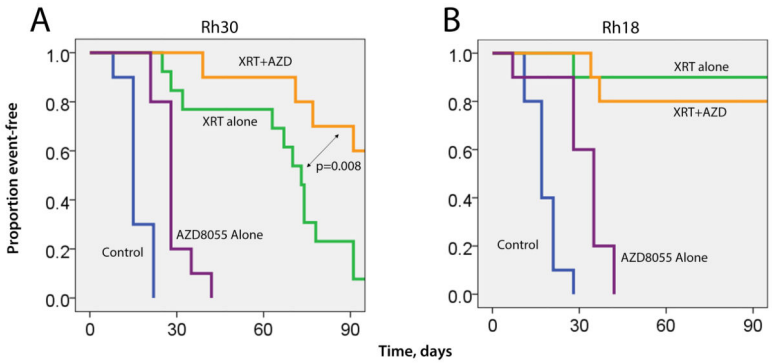

Figure 1.

Preclinical testing results of concurrent AZD8055 and radiotherapy. Kaplan-Meier event-free survival (EFS) curves of the preclinical testing groups: no-treatment [blue]; AZD8055 alone (10mg/kg daily for 3 weeks) [purple]; radiotherapy alone (20 Gy in 10 fractions for 2 weeks) [green]; and combined treatment (3 weeks AZD8055 daily, last 2 weeks with concurrent 2 Gy fractions) [orange]. **A:** EFS curves of mice bearing Rh30 xenografts. The addition of AZD8055 conferred a marginal EFS benefit over no treatment (29 versus 16 days, ($p<0.009$). Those receiving radiotherapy had significant improvements in EFS, compared to no-treatment and AZD8055-alone groups (all $p\leq0.009$. The addition of AZD8055 to radiotherapy significantly improved EFS rate compared to those receiving radiotherapy alone. The median EFS time was 73 days in the radiotherapy alone group and could not be determined in the combined treatment group (> 91 days), $p<0.008$. **B:** EFS curves of mice bearing Rh18 xenografts. The addition of AZD8055 conferred a marginal EFS benefit over no treatment (31 versus 18 days, ($p=0.001$). Those receiving radiotherapy had significant improvements in EFS, compared to no-treatment and AZD8055-alone groups (all $p<0.001$), with mean survival times estimated to be >91 days (median could not be determined). The addition of AZD8055 to radiotherapy did not improve EFS rate compared to those receiving radiotherapy alone.

NIH-PA Author Manuscript
NIH-PA Author Manuscript
NIH-PA Author Manuscript

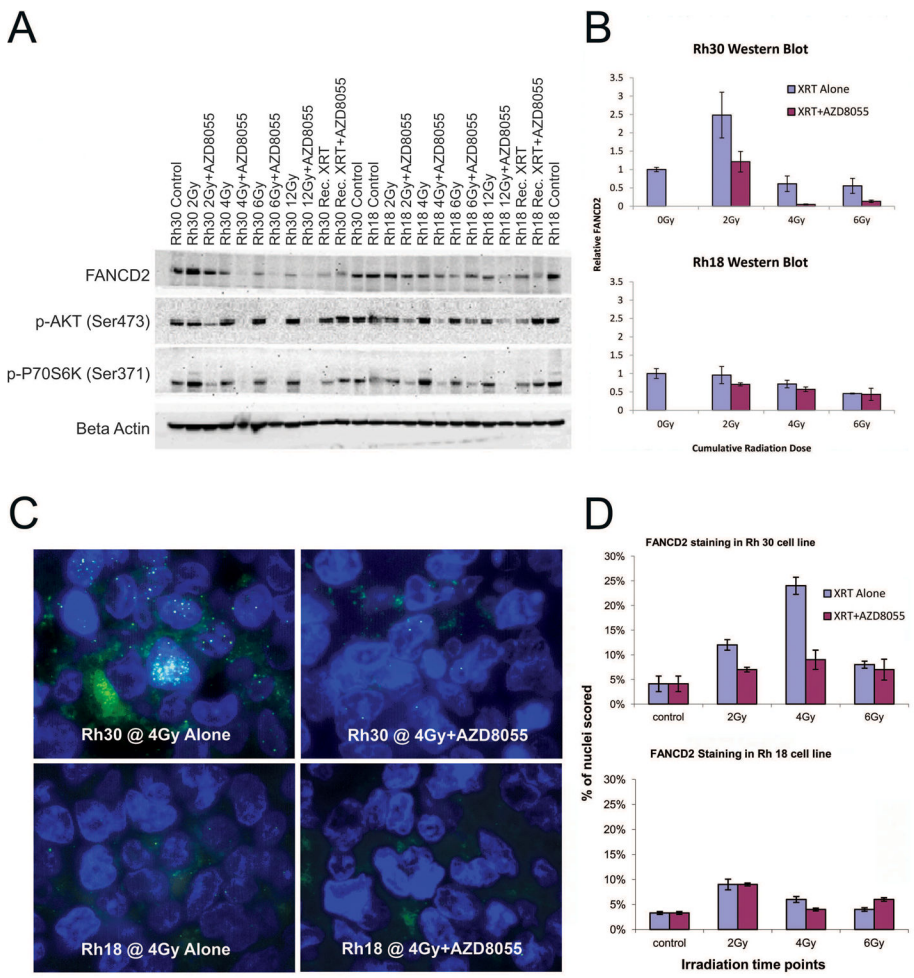

Figure 2.

Xenograft analysis. **A:** Immunoblot analysis of FANCD2 expression and mTOR pathway activation in xenograft samples during radiotherapy with and with and without concurrent AZD8055. Xenografts were harvested for molecular analysis before treatment commenced (control) and 30–60 minutes after 2 Gy daily XRT doses on Days 1, 2, 3, and 8, corresponding to cumulative doses of 2, 4, 6, and 12 Gy and at recurrence (Rec.) with or without concurrent AZD8055. In both lines, mTOR kinase inhibition by AZD8055 is verified (lower phospho-Akt and phospho-P70S6K levels). Rh30 (ARMS), demonstrates a more rapid increase in FANCD2 expression after 2 Gy and a greater amount of suppression by AZD8055 throughout the treatment course. With Rh18 (ERMS), AZD8055 appears to alter the FANDCD2 expression to a lesser degree at each radiation dose level. **B.** These observations were verified by photometrically quantifying FANCD2 levels and normalizing to beta-actin as well. For each sample, a normalization value was determined by dividing the FANCD2 density by the Beta Actin density. This was done for two separate immunoblot experiments. Standard deviation values were determined for each sample's normalized values. Each normalized value was then renormalized relative to the 0Gy control and plotted. NOTE: Each immunoblot lane represents 3–5 pooled biologic replicates in equal proportion. Samples were excluded from pooling if there was inadequate/degraded protein

NIH-PA Author Manuscript

NIH-PA Author Manuscript

NIH-PA Author Manuscript

extracted from xenograft sample. **C:** Photomicrographs of FANCD2 functional foci formation assay in xenograft samples during radiotherapy with and with and without concurrent AZD8055. All samples were harvested from mouse flanks 30–60 minutes after the second 2-Gy daily treatment. Representative photomicrographs of FANCD2 foci staining in: Rh18 xenograft treated with radiation alone, Rh18 xenograft treated with concurrent radiation and AZD8055, Rh30 xenograft treated with radiation alone, and Rh30 xenograft treated with concurrent radiation and AZD8055. **D:** The triplicate average percentage of nuclei positive for activated FANCD2 foci in Rh18 and Rh30 treated with radiation with or without concurrent AZD8055.

NIH-PA Author Manuscript
NIH-PA Author Manuscript
NIH-PA Author Manuscript

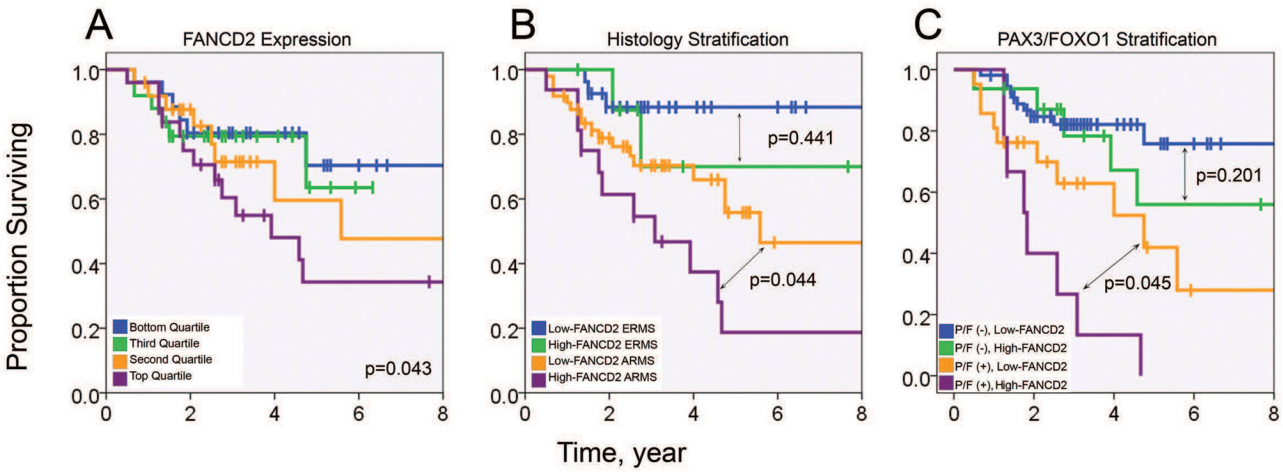

Figure 3.

The prognostic impact of quartile FANCD2 mRNA expression in clinically-annotated Affymetrix U133 Plus 2 gene expression profiles of 101 rhabdomyosarcoma patients. **A:** Kaplan-Meier survival curves of patients when stratified by FANCD2 quartile. Those within the top quartile exhibited the worst outcome with a 5.1year mean survival time, compared to the 8.7 mean survival time in the quartile with the lowest FANCD2 expression. The intermediate quartiles had mean survival times of 5.0–6.3 years (p=0.043, log-rank) **B:** Kaplan-Meier survival curves of patients analyzing the prognostic impact of the top FANCD2 quartile when stratified by histology (ARMS versus ERMS). Within the ARMS subtype, the top quartile of FANCD2 had a mean survival time of 4.0 years while those with lower quartiles had 6.9 years (p=0.044, log rank). **C:** Kaplan-Meier survival curves analyzing the prognostic impact of the top quartile of FANCD2 mRNA expression when stratified by PAX3/FOXO1 translocation status. Patients harboring the PAX3/FOXO1 fusion gene and the top quartile of FANCD2 expression had an exceptionally poor outcome, with a mean survival time of only 2.3 years. The fusion-positive patients had a mean overall survival time of 4.5 years (p=0.045, pairwise log-rank). The dually negative group experienced the best outcome, with a mean survival time of 9.2 years, while non-translocated patients with a top-quartile FANCD2 expression status exhibited an intermediate 6.9-year mean survival time, though on pairwise comparisons, this was not statistically significantly different. However, the overall survival trend across these three stratification groups (dually positive, dually negative and one factor-only) was highly significant (p<0.001, log-rank).

NIH-PA Author Manuscript
NIH-PA Author Manuscript
NIH-PA Author Manuscript

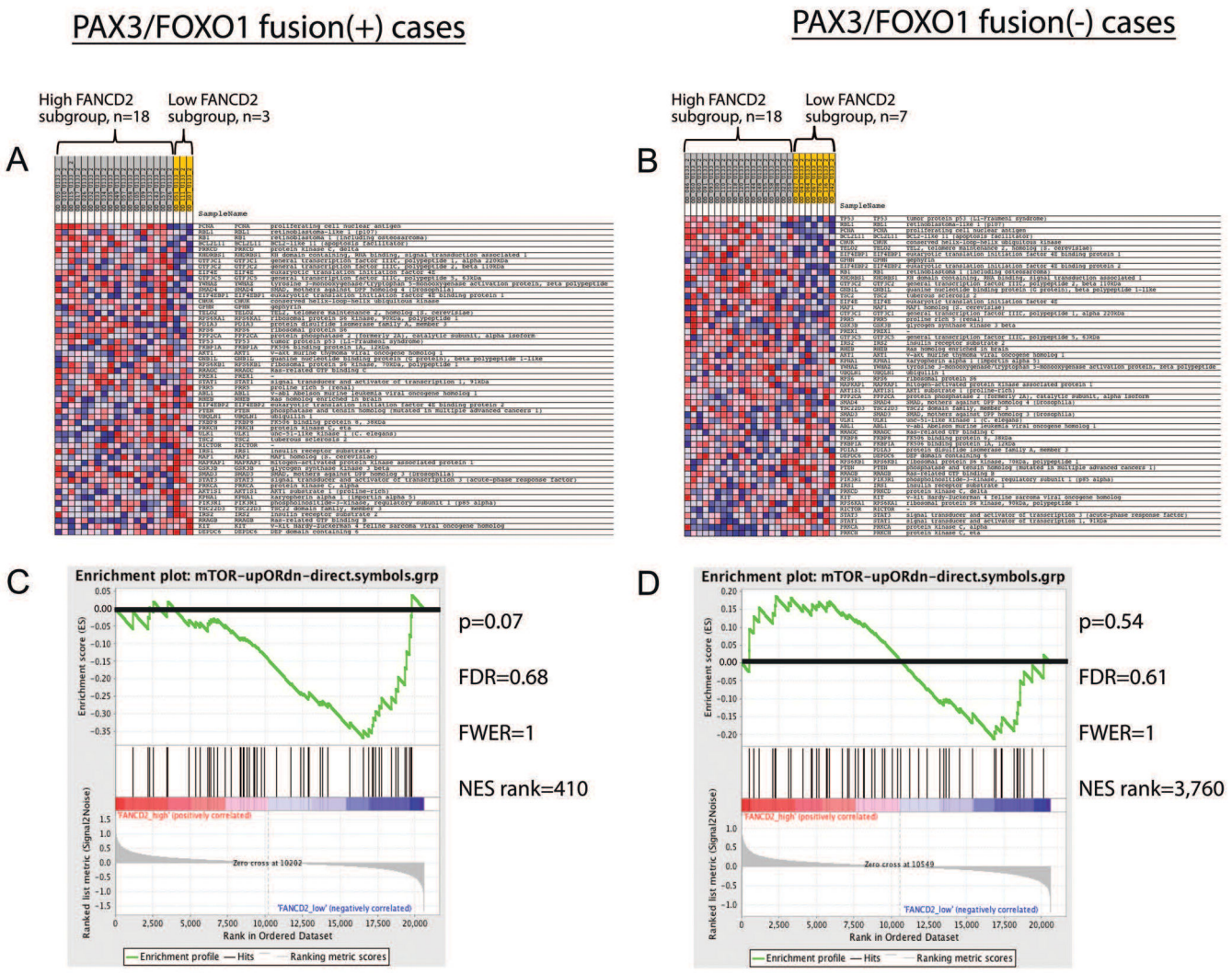

Figure 4.

mTOR-associated Gene Set Enrichment Analysis (GSEA) (23–24) in clinically-annotated Affymetrix U133 Plus 2 gene expression profiles of 101 rhabdomyosarcoma patients. **A.** Heat map of the k-means clustering results of mTOR associated genes in high (n=18) versus low (n=3) FANCD2 mRNA expression cases (4.3-fold difference) in the PAX3/FOXO1 fusion gene-positive subgroup (complete gene list and tabular values can be found in Supplementary Table S3). To isolate FANCD2 associations, the intermediate FANCD2 level subset was omitted from analysis of the fusion-positive cases (n=13). **B.** Heat map of the k-means clustering results of mTOR associated genes in high (n=18) versus low (n=7) FANCD2 mRNA expression cases (4.3-fold difference) in the fusion-negative subgroup (complete gene list and tabular values can be found in Supplementary Table S3). To isolate FANCD2 associations, the intermediate FANCD2 level subset was omitted from analysis of the fusion-negative cases (n=33). **C.** Gene enrichment plot of mTOR-associated genes within the PAX3/FOXO1 fusion gene-positive subgroup. A non-random, inverse enrichment of mTOR associated gene transcripts with FANCD2 transcripts is observed within this subgroup. **D.** Gene enrichment plot of mTOR-associated genes within the fusion-negative

subgroup. There is a near equal distribution of direct and inversely enriched genes, indicative of a random association of mTOR-associated transcripts to FANCD2 in this subgroup.

NIH-PA Author Manuscript
NIH-PA Author Manuscript
NIH-PA Author Manuscript

NIH-PA Author Manuscript

NIH-PA Author Manuscript

NIH-PA Author Manuscript

Table 1

Multivariate Cox Model of Initial Patient Set.

	Initial Patient Set, n=86		
Factor	**HR**	**95% CI**	**P-value**
Unfavorable site	--	--	--
PAX3/FOXO1+High FANCD2*	3.2	1.5–7.5	0.033
Metastatic disease	3.1	1.6–7.6	0.003
PAX3/FOXO1 translocation	2.4	1.0–5.78	0.051

Factors included in the model, but not significant: histology (ARMS versus ERMS), size of primary (5 cm cut-off), nodal status, translocation status, FANCD2 expression. Seventy-six cases had known status of each of these factors and comprised the Cox model.

* rhabdomyosarcoma cases with PAX3/FOXO1 translocation and top quartile FANCD2 mRNA; HR, Hazard Ratio; 95% CI, 95% confidence interval.

NIH-PA Author Manuscript NIH-PA Author Manuscript NIH-PA Author Manuscript

Table 2

Spearman rank analysis of molecular and clinical markers.

		FANCD2	p-p70S6K	P-Akt	PAX3	PAX7	ARMS	Tumor size >5 cm	Node- positive	Metastatic
All Cases*										
FANCD2	Correlation Coefficient		0.35	0.19	0.29	−0.15	0.09	−0.14	0.04	0.11
	P		<0.001	0.051	0.003	0.141	0.337	0.184	0.744	0.275
	N		107	107	104	104	110	94	87	93
p-p70S6K	Correlation Coefficient	0.35		0.36	0.30	0.16	0.37	−0.11	0.09	0.08
	P	<0.001		<0.001	0.002	0.091	<0.001	0.299	0.385	0.423
	N	107		115	108	108	114	97	90	95
p-Akt	Correlation Coefficient	0.19	0.36		0.18	0.21	0.30	−0.09	0.08	0.09
	P	0.051	<0.001		0.058	0.029	0.001	0.402	0.459	0.371
	N	107	115		110	110	116	98	91	96
PAX3/FOXO1 Fusion Positive Cases										
FANCD2	Correlation Coefficient		0.60	0.14						
	P		0.001	0.482						
	N		27	27						
p-p70S6K	Correlation Coefficient	0.60		0.40						
	P	0.001		0.028						
	N	27		30						
p-Akt	Correlation Coefficient	0.14	0.40							
	P	0.482	0.028							
	N	27	30							
Fusion Negative Cases										
FANCD2	Correlation Coefficient		0.17	0.12						
	P		0.200	0.343						

NIH-PA Author Manuscript
NIH-PA Author Manuscript
NIH-PA Author Manuscript

		FANCD2	p-p70S6K	P-Akt	PAX3	PAX7	ARMS	Tumor size >5 cm	Node- positive	Metastatic
	N		60	60						
p-p70S6K	Correlation Coefficient	0.17		0.24						
	P	0.200		0.050						
	N	60		65						
p-Akt	Correlation Coefficient	0.12	0.24							
	P	0.343	0.050							
	N	60	65							

*All Cases: Spearman rank correlation screen of FANCD2, p-P70S6K, p-Akt and established prognostic clinical factors of all cases (significant correlations are highlighted). **RAX3/FOXO1 Fusion Positive Cases:** Spearman rank correlation screen of FANCD2, p-P70S6K, and p-Akt of cases with the PAX3/FOXO1 fusion gene. **Fusion Negative Cases**: Spearman rank correlation screen of FANCD2, p-P70S6K, and p-Akt of cases without the fusion gene.